ARCHIVES of FOUNDRY ENGINEERING

ISSN (2299-2944)
Volume 2026
Issue 1/2026

97 – 104

11/1

10.24425/afe.2026.157974

Published quarterly as the organ of the Foundry Commission of the Polish Academy of Sciences

Evaluation of the Accuracy of Mg Alloy Castings Manufactured by Rapid Ceramic Method Using Printed Models

A. Dmitruk *, K. Naplocha, N. Łobacz-Raźny
Department of Lightweight Elements Engineering, Foundry and Automation, Faculty of Mechanical Engineering, Wrocław University of Science and Technology, Poland
* Corresponding author: E-mail address: anna.dmitruk@pwr.edu.pl

Received 13.08.2025; accepted in revised form 19.12.2025; available online 30.03.2026

Abstract

This study discusses the accuracy of manufacturing honeycomb-based cellular structures cast from Mg alloy (AZ91) by rapid ceramic method using 3D printed models. 3D scanning was used to assess the processing shrinkage occurring during both stages of the manufacturing process (3D printing in fused deposition modelling (FDM) or digital light processing (DLP) technologies and rapid ceramic method). Bioresorbable scaffolds made of Mg alloys can be used, for example, in the construction of bone implants. A method of controlling the biodegradation rate of these materials by applying protective plasma electrolytic oxidation (PEO) coatings was also presented. Phosphate buffered saline (PBS) solution was applied as a measure to evaluate the corrosion resistance of produced structures in physiological conditions. Samples with a PEO oxide coating were proved to be the most promising ones, because the pH and mass change observed for them was the lowest among all tested materials (as cast, sand-blasted, PEO-coated).

Keywords: Rapid ceramic method, 3D scanning, Honeycomb, Scaffolds, Magnesium casting

1. Introduction

Magnesium and its alloys have become a promising solution to replace commonly used biomaterials in implant-related applications [1-3]. This material offers not only biocompatibility, but also provides anti-bacterial and anti-inflammatory properties [4]. Moreover, magnesium is osteoconductive and exhibits mechanical properties (especially Young's modulus) closer to those of natural bones in comparison to conventionally utilized stainless steel, titanium or cobalt-chromium alloys [4-6]. The latter feature helps to avoid the problem of "stress shielding" resulting with over-stiffening of repaired joints, leading to the implants loosening and degradation of the surrounding bone tissue [7]. Cellular scaffolds are often applied for the same purpose – to weaken the implant for it to be comparable with the performance of human bones [8]. Although casting methods can be a suitable way to manufacture such porous structures, liquid-phase processes are strictly connected with significant shrinkage. Therefore a careful quality assessment is required to ensure the proper dimensions are obtained. Another limitation of using magnesium corresponds to its rapid bioresorption, that can occur even during the foreseen exploitation time of the implant [9-10]. In order to mitigate this risk several solutions are possible: alloying of Mg with Zn, Ca, Mn, Sr, RE etc., or deposition of protective coatings postponing the degradation process (e.g. micro-arc oxidation (MAO), polydopamine or graphene-based coatings, chemical etching, electrochemical deposition etc.) [11]. Thus such non-toxic implants are able to fulfil their function for a required period, being

controllably and gradually dissolved, without the necessity of an additional removal operation [12].

In this paper, the combined technologies of FDM (Fused Deposition Modelling) or DLP (Digital Light Processing) with rapid ceramic method (elsewhere referred to as lost wax or investment casting) with AZ91 alloy were hereby proposed to produce honeycomb-type structures. The comparative assessment of the 3D printing and casting accuracy was conducted using the 3D scanning method. A PEO oxide coating was deposited on the selected samples to reduce the biodegradation rate. Its effectiveness was tested during PBS immersion tests for 24 h. It has to be highlighted that the AZ91 alloy was chosen for this study because of the good castability and corrosion resistance of this material. This material was meant to serve as a preliminary reference for future studies. Nevertheless, it possesses a relatively high content of Al that is harmful for the human body, being known to induce neurodegenerative diseases such as multiple sclerosis or Alzheimer's or Parkinson's diseases [13]. In spite of this it should not be applied in biomedical implants. Therefore, in future studies an emphasis will be put on searching for a less or non-toxic alternative: starting with AZ31 alloy (containing only 3% Al instead of 9%) through to completely aluminium-free magnesium-based alloys such as Mg-Zn or Mg-Zn-Ca.

2. Methodology

The process is shown in Figure 1. Test samples were firstly designed with the use of Autodesk Inventor Professional software. They were cylindrical with internal cores possessing a cellular honeycomb-type structure enveloped with an outer solid wall. Similar structures were also applied in [14] showing mechanical properties corresponding to the ones of natural (cortical or trabecular) bones. The shorter diagonal of the hexagon cell equalled 5 mm. All of the structures were characterized with a wall thickness of 0.6 mm, height of 10 mm and external diameter of approx. 30 mm (precise resulting dimension of the design is 30.023 mm). Next, the samples destined to be printed with the use of two additive manufacturing technologies – namely FDM and DLP, were sliced respectively with a Prusa Slicer and Lychee Slicer into .gcode files. Afterwards, they were 3D printed using Prusa i3 MK3S and Anycubic Photon Mono X printers. Three different printing materials were utilized: Fiberlogy Easy PLA filament, Bluecast Original X5 and Castable LCD Series Castable Wax photocurable resins. DLP-printed samples were additionally washed and cured with an Anycubic Wash & Cube machine. Prepared samples were used as patterns for rapid ceramic method with AZ91 magnesium alloy (9% Al, 0.13% Mn, 0.7% Zn, Mg – rest). Plaster moulds were prepared on this basis with Ransom & Randolph Plasticast gypsum. The next stage, the burn-out cycle, was performed with a maximum temperature of 730°C. It led to the mould's dehydration and strengthening combined with full removal of the model tree (melting of wax gating system and gasification of polymer patterns). After the burning out of the plaster moulds, they were filled with molten AZ91 alloy under low pressure and protective gas shielding. Microscopic analysis was performed by the means of a TM3000 scanning electron microscope with EDS analyser. Samples were further analysed without (as cast) and with two kinds of surface treatment: sand-blasting and PEO coating. Dimensional accuracy, indicating processing shrinkage present both during 3D printing and rapid ceramic processes, was comparatively assessed with the use of a SHINING 3D® Einscan SP V2 3D scanner.

The samples for PEO treatment were cleaned in 4% NaOH solution for two minutes, rinsed in water and sand-blasted. For the PEO coating, a sanded sample was rinsed in ethanol to degrease the surface and dried in room temperature airflow. The electrolyte comprised 5 g/L KOH and 7.65 g/L $Na_3PO_4 \cdot H_2O$ (3.3 g/L Na_3PO_4). The HI98130 (Hanna instruments, Romania) was used to examine the pH of the electrolyte, giving a value of 12.7. A custom-made semi-industrial power supply provided by Micro-Arc S.C. (Poland) was used for PEO treatment. The process took 2000 seconds and consisted of two steps in order to achieve the plasma discharges on the complex sample's surface. The steps are described below in Table 1. The electrolyte temperature was kept at around 15°C.

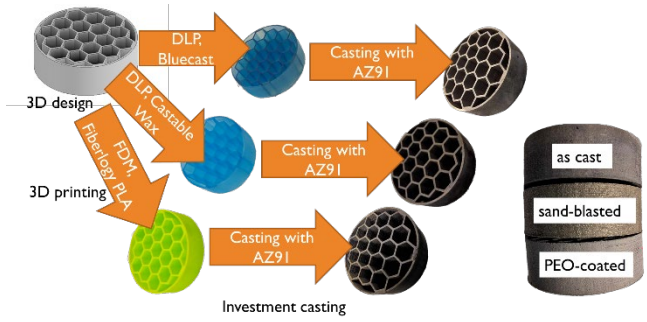

Fig. 1. The utilized manufacturing process

Table 1.
Parameters of the applied PEO process

Steps	Time of step duration (s)	Frequency (Hz); positive:negative current ratio (ms)	Set current densities (positive:negative) (mA/cm^2)	Final voltage (V)
I	990	1000; 0.7:0.3	130:100	187
II	1010	1000; 0.7:0.3	330:210	315

PBS immersion tests were conducted to evaluate the corrosion resistance in physiological conditions of all kinds of the elaborated structures: as cast, sand-blasted and PEO-coated. Mass gain and pH changes were observed during immersion after 2 h, 4 h, 6 h and 24 h. Corrosion products formed at the surface were subjected to microscopic analysis.

3. Results and discussion

The manufactured cellular structures were subjected to the comparative assessment of dimensional accuracy of the production process. It considered each of its stages: 3D-printing and rapid ceramic method, for various materials for the patterns preparation. The results of the regular measurements done with the use of a calliper, as well as those taken by means of 3D scanning are gathered in Tables 2 and 3, respectively for the patterns and castings. Average shrinkage levels were also calculated. The

greatest deviations from the designed values for cells diagonals and outer diameters were stated for the patterns 3D-printed with DLP and Bluecast resin (DLP2) with a shrinkage of approx. 6%. The results for the remaining two materials (Fiberlogy PLA (FDM) and Castable Wax resin (DLP1)) were comparable in terms of the cell's accuracy (shrinkage of 1.1-1.4%), but FDM offered better fit for the external diameter (only 0.33% of shrinkage). Analogous results were obtained for castings. As only total shrinkage in relation to the designed dimensions was considered, the shrinkage in each case is greater than it was for the first stage. The total shrinkage of the cell's diagonal after both processes equalled 2.13%, 1.35% and 7.65% respectively for FDM, DLP1 and DLP2. For the same order of samples the average total shrinkage of the outer diameter was: 0.68%, 1.93% and 6.21%. Exemplary measurements from the 3D scanning process obtained using EXScan S software are shown in Figure 2.

Table 2.
Assessment of the 3D-printed patterns accuracy – measured and scanned values and calculated shrinkage level

Pattern - FDM, Fiberlogy PLA, FDM												
Pattern - FDM, Fiberlogy PLA	3D design	measured 1	measured 2	measured 3	standard deviation	mean value	scan 1	scan 2	scan 3	standard deviation	mean value	shrinkage [%]
Cell [mm]	5	4.95	4.94	4.97	0.01	4.95	4.862	5.027	4.95	0.067	4.946	1.07
Outer diameter [mm]	30.023	29.97	30.10	29.91	0.08	29.99	29.764	30.072	29.939	0.126	29.925	0.33
Pattern – DLP, Castable Wax, DLP1												
Pattern – DLP, Castable Wax	3D design	measured 1	measured 2	measured 3	standard deviation	mean value	scan 1	scan 2	scan 3	standard deviation	mean value	shrinkage [%]
Cell [mm]	5	4.98	4.90	4.95	0.03	4.94	4.937	4.908	4.946	0.016	4.930	1.39
Outer diameter [mm]	30.023	29.78	29.73	29.80	0.03	29.77	29.424	29.871	29.866	0.210	29.720	1.01
Pattern - DLP, Bluecast, DLP2												
Pattern - DLP, Bluecast	3D design	measured 1	measured 2	measured 3	standard deviation	mean value	scan 1	scan 2	scan 3	standard deviation	mean value	shrinkage [%]
Cell [mm]	5	4.75	4.77	4.75	0.01	4.76	4.664	4.707	4.702	0.019	4.691	6.18
Outer diameter [mm]	30.023	28.22	28.02	28.27	0.11	28.17	28.239	28.383	28.192	0.081	28.271	5.83

Table 3.
Assessment of the castings accuracy – measured and scanned values and calculated shrinkage level

Casting - FDM, Fiberlogy PLA, FDM												
Casting - FDM, Fiberlogy PLA	3D design	measured 1	measured 2	measured 3	standard deviation	mean value	scan 1	scan 2	scan 3	standard deviation	mean value	shrinkage [%]
Cell [mm]	5	4.88	4.94	4.93	0.03	4.92	4.859	4.907	4.914	0.024	4.893	2.13
Outer diameter [mm]	30.023	29.59	29.79	29.52	0.11	29.63	29.621	30.013	29.827	0.160	29.820	0.68
Casting - DLP, Castable Wax, DLP1												
Casting - DLP, Castable Wax	3D design	measured 1	measured 2	measured 3	standard deviation	mean value	scan 1	scan 2	scan 3	standard deviation	mean value	shrinkage [%]
Cell [mm]	5	4.90	4.91	4.94	0.02	4.92	4.935	4.881	4.982	0.041	4.933	1.35
Outer diameter [mm]	30.023	29.66	29.56	29.57	0.04	29.60	29.464	29.377	29.494	0.050	29.445	1.93
Casting - DLP, Bluecast, DLP2												
Casting - DLP, Bluecast	3D design	measured 1	measured 2	measured 3	standard deviation	mean value	scan 1	scan 2	scan 3	standard deviation	mean value	shrinkage [%]
Cell [mm]	5	4.71	4.73	4.77	0.02	4.74	4.602	4.586	4.664	0.034	4.617	7.65
Outer diameter [mm]	30.023	27.04	28.00	28.05	0.46	27.70	28.252	28.212	28.016	0.103	28.160	6.21

Due to the fact that the casting obtained with the use of the PLA pattern showed the closest dimensions to the designed ones it was

chosen for further examinations. Additionally, a porous layered structure may be useful for the bone cells attachment and tissue ingrowth, which may be another benefit [15]. Nevertheless, the resin samples will be subjected to the dimension optimization process in future studies. The views of the top surfaces of all of three types of samples are shown in Figure 3. The as cast sample (Fig. 3a) exhibits layered topology originating from the FDM printing process, reflecting subsequently deposited layers of the filament. This feature cannot be noticed in Fig. 3b and 3c, because of the cutting of the tops of these layers by sand-blasting operation. Uniformly porous morphology, typical for PEO coating, can be seen in Fig. 3c.

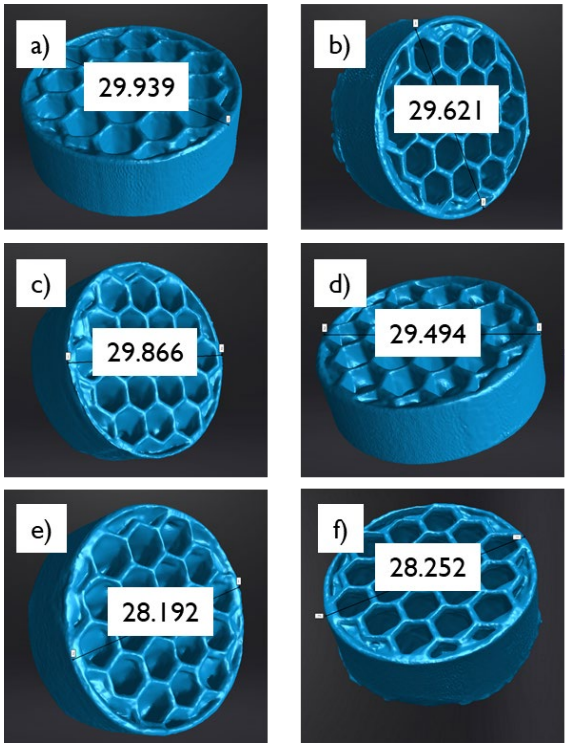

Fig. 2. Exemplary measurements from 3D-scanned structures: a) FDM pattern, b) FDM casting, c) DLP1 pattern, d) DLP1 casting, e) DLP2 pattern, f) DLP2 casting,

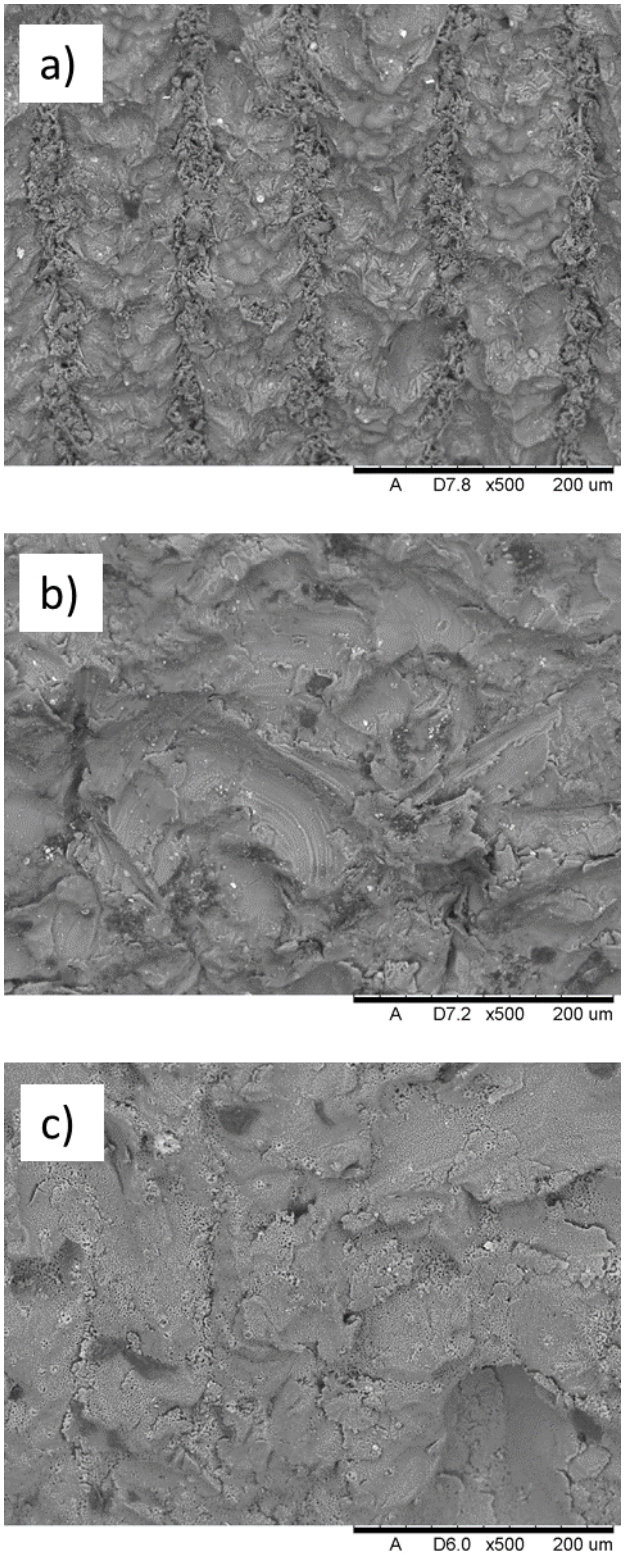

Fig. 3. SEM view of the surface of castings based on FDM patterns: a) as cast, b) sand-blasted, c) PEO-coated

Figure 4 focuses on PEO-treated sample, showing a general view of the cell walls' crossing and exemplary results of aerial EDS analysis of the PEO coating, confirming the formation of a magnesium oxide layer. The views of the chosen (originated from FDM 3D-printed patterns) samples before and during the PBS immersion test are presented in Figure 5.

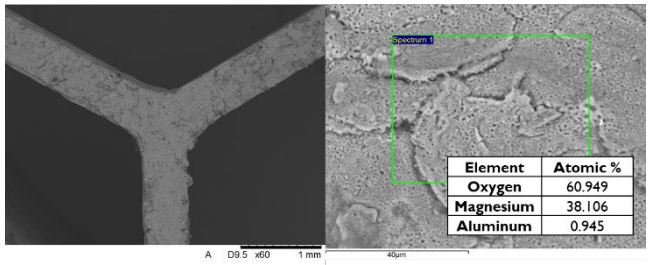

Fig. 4. PEO-coated sample: general view with exemplary EDS analysis

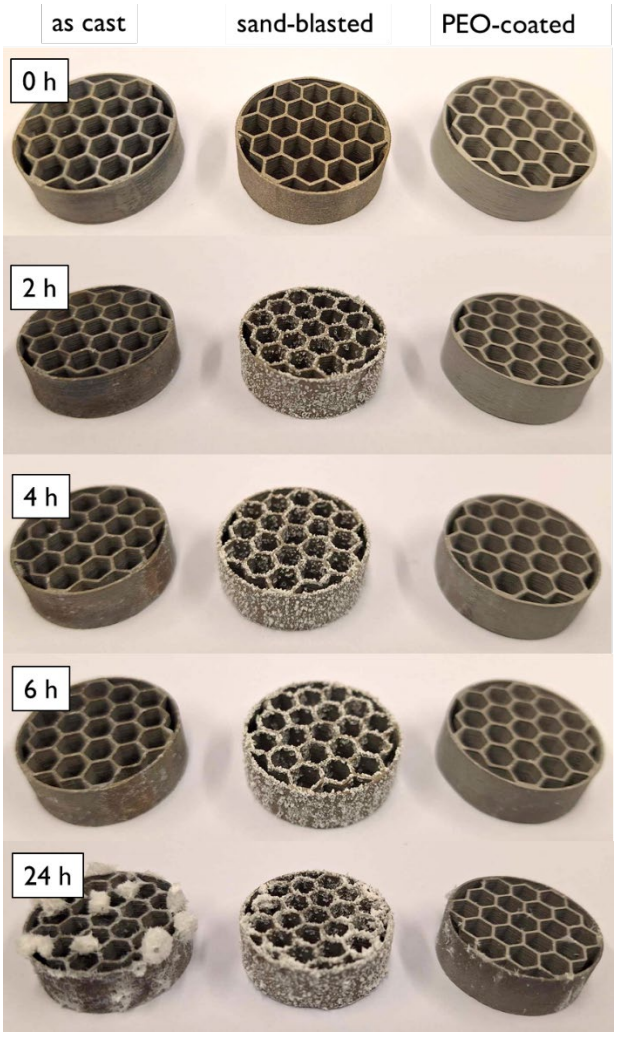

Fig. 5. View of the set of samples (as cast, sand-blasted, PEO-coated) before and after 2 h, 4 h, 6 h and 24 h of immersion in PBS

PEO-coated samples could be recognized even before PBS treatment, as it is significantly brighter due to the presence of the coating. The PEO coating consisted of two layers: an inner, dense one and an outer, highly porous one [16]. Sand-blasted samples, deprived of the natural oxide layer or the PEO-deposit, reacted right away after being put in the PBS solution. A notable number of bubbles resulting from the severe and abrupt oxidation could be noticed from the start of the test. After 2 hours of immersion, the powder-like white layer was observed on its surface, while other two samples remained unaffected. First, slightly visible precipitations were formed on the as cast sample after 4 h. After 6 h, it can be stated that these corrosion products grow for the first two types of samples, keeping the PEO sample still unchanged. It is only at the end of the test, after 24 h, that the PEO-coated samples started to show any effects of the corrosion. White deposits formed on as-cast and sand-blasted samples were greatly thickened. Additionally, on the as cast sample some point clusters of agglomerated corrosion products were present.

The mass change fraction depicted in Figure 6a highlights the stability of the PEO-coated sample. The mass gain observed after 24 h of immersion in PBS for the as cast sample was averaged to 1.33%, while for sand-blasted structures it equalled 3.55%. Analogous outcomes were reported for pH observations in Figure 6b – the most stable behaviour corresponded to PEO-coated AZ91 alloy. In each case, the pH moved from physiological upwards, up to 9.7, 10.7 and 11.8 for the PEO-coated, as cast and sand-blasted samples respectively. While a small rise of pH might be favourable for the proliferation of bone cells [17], the change observed even for the PEO-coated samples may be too high, thus further refinement of these layers is required (e.g. additional sealing of potential discontinuities or cracks). Such operation is often described by other researchers worldwide [16, 18]. Too extreme alkaline conditions can lead to the detrimental effect of bone erosion [19].

Each of the evaluated corrosion products, as concluded in the EDS results given in Table 4 consisted mainly of O and Mg, with some residuals from PBS (e.g. Na, P, K). Among these products, differing morphologies of these formed substances could be noticed (see Figure 7). Fig. 7a and Fig. 7c show fibrous products, while in Fig. 7b a powder-like crystal structure was obtained. Formation of rod-shaped degradation products was also stated in [20], where they were identified as magnesium oxides and hydroxides. In this work, the presence of phosphorus was more substantial in the observed fibres, therefore it is believed that these corrosion products may be also composed of magnesium phosphates [21]. Apart from the above described outcomes, PEO coating can also be beneficial in another way: its porous character may increase the activity of osteoblasts enhancing proliferation at the same time, but it also significantly limits the amount of released hydrogen during bioresorption [22]. Once again, it has to be highlighted that for actual medical purposes a different Mg alloy, free of Al, should be selected.

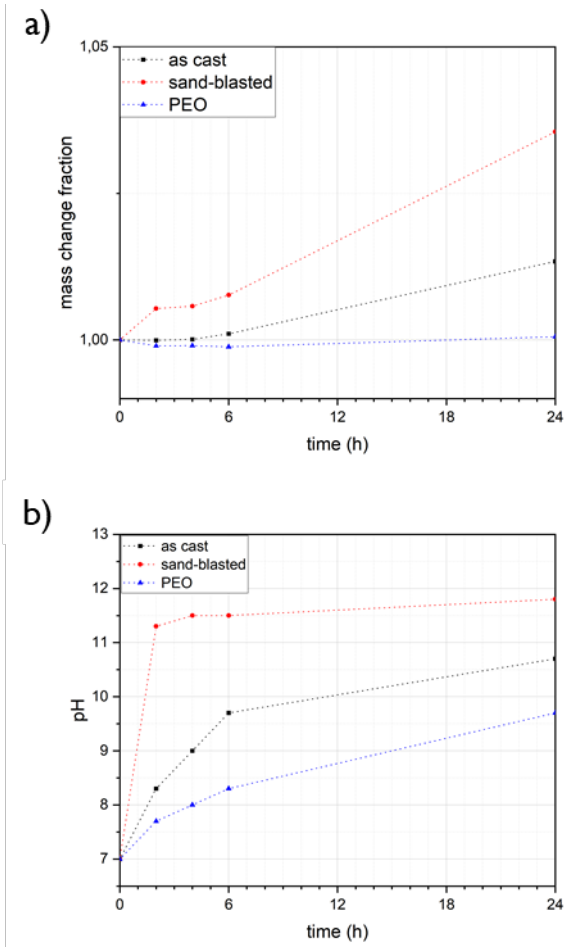

Fig. 6. Degradation test in PBS: a) mass change fraction vs time, b) pH vs time

Table 4.
EDS analysis of corrosion products for as cast, sand-blasted and PEO-coated samples after 24 h immersion in PBS

As cast		Sand-blasted		PEO-coated	
Element	**Atomic %**	**Element**	**Atomic %**	**Element**	**Atomic %**
O	70.785	O	69.677	O	67.034
Na	4.200	Na	1.358	Na	5.703
Mg	8.936	Mg	22.088	Mg	9.677
Al	0.854	Al	0.453	P	11.490
P	10.872	P	2.209	Cl	1.808
K	4.354	Cl	4.215	K	4.288

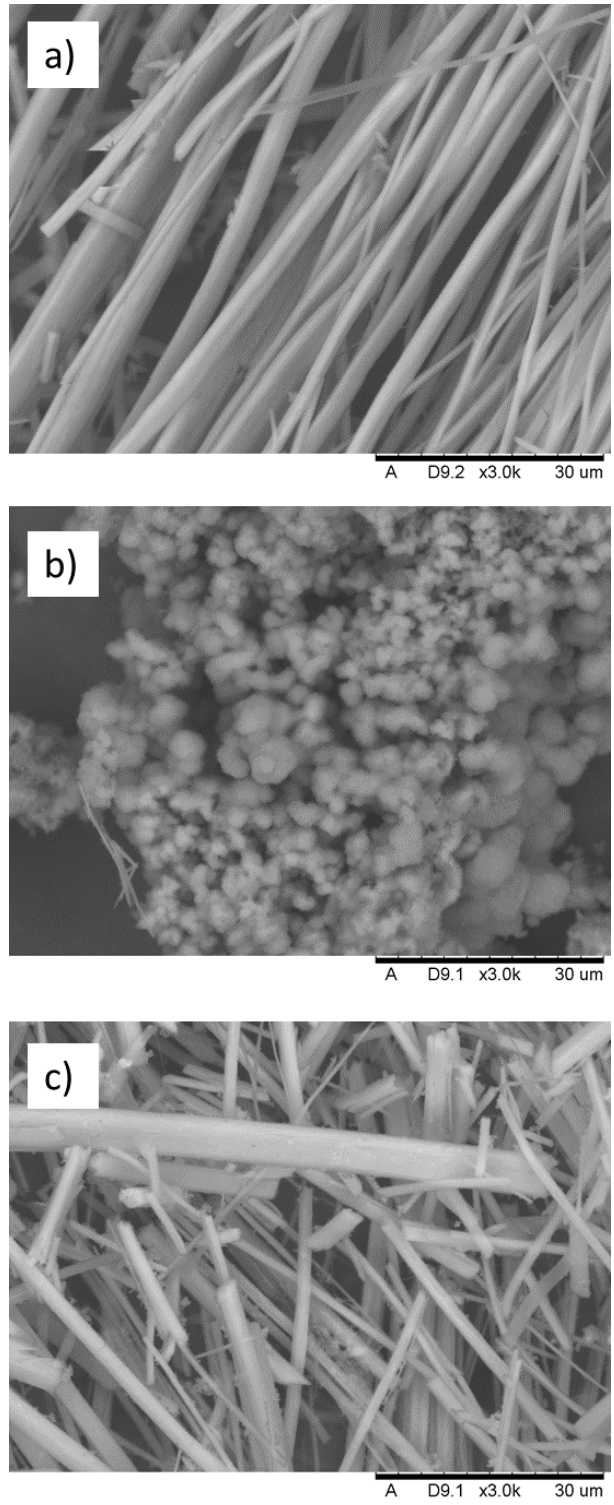

Fig. 7. SEM view of the corrosion products formed on the surface of castings based on FDM patterns after PBS degradation tests for the following samples: a) as cast, b) sand-blasted, c) PEO-coated

4. Conclusions

The following main conclusions of the study may be drawn:

- Rapid ceramic method based on polymer 3D-printed patterns could be successfully applied for the fabrication of complex thin-walled structures from Mg alloy,
- A 3D scanning technique was suitable for the comparative assessment of the castings quality and dimensional accuracy. The results for Fiberlogy Easy PLA filament and Castable Wax resin were comparable with a slight advantage of the first option (total shrinkage of hexagonal cell diagonal of 2.13%, 1.35% and 7.65% and total shrinkage of outer diameter of 0.68%, 1.93% and 6.21% respectively for FDM, DLP1 and DLP2),
- Sand-blasting smoothed out the surface, depriving it of the layered structure in the case of FDM-based castings. Moreover, it severely lowered the corrosion protection, because of the oxide layer removal,
- The PEO layer inhibited corrosion and protected the AZ91 substrate against the biodegradation in PBS conditions. Despite the fact that the corrosion process was greatly postponed, judging by the observation of mass and pH changes (mass gain of 0.06%, 1.33% and 3.55% after 24 h and pH change up to 9.7, 10.7 and 11.8 for PEO-coated, as cast and sand-blasted samples respectively), it finally occured. This might be caused by any imperfection (e.g. microcracks) within the coating, therefore the application of additional sealing may be needed. When applied it may be beneficial from the point of bioresorbability of the implant and possible recovery of natural tissue in its place,
- Although AZ91 could be used as a reference Mg alloy because of its good castability and corrosion resistance, it also possesses a notable content of toxic aluminium – therefore it is required to further develop these studies in search for an alternative for any implantation materials containing either less or no Al (e.g. AZ31 or Mg-Zn alloys).

Acknowledgements

The presented research results were carried out as part of the research task "Cellular structures cast from Mg alloys for use in bone implants", financed from the pro-quality subsidy for the development of the research potential of the Faculty of Mechanical Engineering, Wrocław University of Science and Technology in the year 2024.

References

[1] Wang, N., Ma, Y., Shi, H., Song, Y., Guo, S. & Yang, S. (2022). Mg-, Zn-, and Fe-based alloys with antibacterial properties as orthopaedic implant materials. *Frontiers in Bioengineering and Biotechnology*. 10, 888084, 1-32. DOI:10.3389/fbioe.2022.888084.

[2] Yavuzyegit, B., Karali, A., De Mori, A., Smith, N., Usov, S., Shashkov, P., Bonithon, R. & Blunn, G(2024). Evaluation of corrosion performance of AZ31 Mg alloy in physiological and highly corrosive solutions. *ACS Applied Bio Materials*. 7(3), 1735-1747. DOI:10.1021/acsabm.3c01169.

[3] Wang, L., He, J., Yu, J., Arthanari, S., Lee, H., Zhang, H., Lou, L., Huang, G., Xing, B., Wang, H. & Shin, K. S. (2022). Review: degradable magnesium corrosion control for implant applications. *Materials*. 15(18), 6197, 1-31. DOI:10.3390/ma15186197.

[4] Uppal, G., Thakur, A., Chauhan, A. & Bala, S. (2022). Magnesium based implants for functional bone tissue regeneration – A review. *Journal of Magnesium and Alloys.* 10(2), 356-386. DOI: 10.1016/j.jma.2021.08.017.

[5] Cabeza, S., Zubiaur, P.P., Garcés, G., Andrade, C. & Adeva, P. (2020). Corrosion behaviour of Mg98.5Nd1Zn0.5 (at. %) alloy in phosphate buffered saline solution. *Metals*. 10(1), 148, 1-16. DOI:10.3390/met10010148.

[6] Dragomir, L., Antoniac, I., Manescu, V., Antoniac, A., Miculescu, M., Trante, O., Streza, A., Cotrut, C.M. & Forna, D. A. (2023). Microstructure and corrosion behaviour of Mg-Ca and Mg-Zn-Ag alloys for biodegradable hard tissue implants. *Crystals*. 13(8), 1213, 1-18. DOI: 10.3390/cryst13081213.

[7] Matias, T.B., Roche, V., Nogueira, R.P., Asato, G.H., Kiminami, C.S., Bolfarini, C., Botta, W.J. & Jorge Jr, A.M. (2016). Mg-Zn-Ca amorphous alloys for application as temporary implant: Effect of Zn content on the mechanical and corrosion properties. *Materials & Design*. 110, 188-195. DOI:10.1016/j.matdes.2016.07.148.

[8] Safavi, S., Yu, Y., Robinson, D.L., Gray, H.A. Ackland, D.C. & Lee, P.V.S. (2023). Additively manufactured controlled porous orthopaedic joint replacement designs to reduce bone stress shielding: a systematic review. *Journal of orthopaedic surgery and research.* 18(1), 42.:10.1186/s13018-022-03492-9.

[9] Ghayad, I.M., Maamoun, M.A., Metwally, W.A., Abd El-Azim, A.N. & El-Baradie, Z.M. (2015). Corrosion control of Mg-Zn implant alloys in simulated body fluid. *Chemistry and Materials Research*, 7(7).

[10] Vignesh, P., Ramanathan, S., Ashokkumar, M. & Ananthi, V. (2024). Biodegradable Mg–3Zn alloy/titanium–hydroxyapatite hybrid composites: corrosion and cytotoxicity evaluation for orthopedic implant applications. *Transactions of the Indian Institute of Metals*. 77(6), 1701-1710. DOI:10.1007/s12666-024-03281-4.

[11] Wei, L., & Gao, Z. (2023). Recent research advances on corrosion mechanism and protection, and novel coating materials of magnesium alloys: a review. *RSC advances.* 13(12), 8427-8463. DOI:10.1039/d2ra07829e.

[12] Fekry, A.M. & Tammam, R.H. (2012). Electrochemical behavior of magnesium alloys as biodegradable materials in phosphate buffer saline solution. *International Journal of Electrochemical Science*. 7(12), 12254-12261.

[13] Petrović, Ž., Šarić, A., Despotović, I., Katić, J. & Petković, M. (2021). Aluminium in dental implants: how to reduce a potential risk to patient's health? *Materials Proceesing*. 6(1), 12, http://doi.org/10.3390/CMDWC2021-09933.

[14] Dmitruk, A., Díaz Lantada, A., Ferraris, S., Łobacz-Raźny, N., Spriano, S. & Naplocha, K. (2024). Investment casting of porous Mg-alloy networks biomechanically tuned for bone implant applications. *The International Journal of Advanced*

Manufacturing Technology. 135(7), 3473-3486. https://doi.org/10.1007/s00170-024-14658-6.
[15] Antoniac, I., Manescu, V., Antoniac, A. & Paltanea, G. (2023). Magnesium-based alloys with adapted interfaces for bone implants and tissue engineering. *Regenerative Biomaterials.* 10, rbad095, 1-61. DOI:10.1093/rb/rbad095.
[16] Li, N., Ling, N., Fan, H., Liang, K., Zhang, J. & Wang, L. (2023). Smart functionalization of PEO coating on AZ31B magnesium alloy by a novel facile one-step sealing method. *Surface and Coatings Technology*. 467, 129674, 1-14. DOI:10.1016/j.surfcoat.2023.129674.
[17] Galow, A.M., Rebl, A., Koczan, D., Bonk, S.M. Baumann, W. & Gimsa, J. (2017). Increased osteoblast viability at alkaline pH in vitro provides a new perspective on bone regeneration. *Biochemistry and Biophysics Reports.* 10*,* 17-25. DOI:10.1016/j.bbrep.2017.02.001.
[18] Fattah-alhosseini, A., Fardosi, A., Karbasi, M. & Kaseem, M. (2024). Advancements in enhancing corrosion protection of Mg alloys: A comprehensive review on the synergistic effects of combining inhibitors with PEO coating. *Journal of Magnesium and Alloys*. 12(2), 465-489. DOI: 10.1016/j.jma.2024.02.001.
[19] Amadasi, A., Camici, A., Sironi, L., Profumo, A., Merli, D., Mazzarelli, D., Porta, D., Duday, H. & Cattaneo, C. (2015). The effects of acid and alkaline solutions on cut marks and on the structure of bone: An experimental study on porcine ribs. *Legal Medicine*. 17(6), 503-508. https://doi.org/10.1016/j.legalmed.2015.10.006.
[20] Khalili, M.A. & Tamjid, E. (2021). Controlled biodegradation of magnesium alloy in physiological environment by metal organic framework nanocomposite coatings. *Scientific Reports*. 11(1), 8645, 1-13. https://doi.org/10.1038/s41598-021-87783-x.
[21] Barberi, J., Saqib, M., Dmitruk, A., Opitz, J., Naplocha, K., Beshchasna, N., Spriano, S. & Ferraris, S. (2024). Characterization of tannic acid-coated AZ31 Mg alloy for biomedical application and comparison with AZ91. *Materials.* 17(2), 343. DOI:10.3390/ma17020343.
[22] Cesarz-Andraczke, K. & Kazek-Kęsik, A. (2020). PEO layers on Mg-based metallic glass to control hydrogen evolution rate. *Bulletin of the Polish Academy of Sciences: Technical Sciences*. 68(1), 119-124. DOI:10.24425/bpasts.2020.131841.